Hindawi
International Journal of RF and Microwave Computer-Aided Engineering
Volume 2023, Article ID 4814376, 9 pages
https://doi.org/10.1155/2023/4814376

Research Article

Asymmetric Coplanar Strip- (ACS-) Fed Side Edge Panel MIMO Antenna for IoT and 5G Applications

Issmat Shah Masoodi,[1] **Javaid A. Sheikh**,[2] **Zahid A. Bhat**,[2] **Shazia Ashraf**,[2] **and Shabir A. Parah**[2]

[1]*Department of Electronics and Communication, Islamic University of Science and Technology, Awantipora, India*
[2]*Department of Electronics and IT, University of Kashmir, Hazratbal, Srinagar, India*

Correspondence should be addressed to Javaid A. Sheikh; sheikhjavaid@uok.edu.in

Received 23 December 2022; Revised 20 October 2023; Accepted 30 October 2023; Published 28 December 2023

Academic Editor: Ashish Bagwari

For future wireless high-speed wireless applications, the antenna design plays an indispensable role. Electrical compactness has been challenging over the years among the research fraternity. Hence, this paper proposes an electrically compact and miniaturized asymmetric coplanar strip- (ACS-) fed MIMO to bridge this research gap. In MIMO antennas, two electrically small antennas are used and are placed on the edges of the smartphone. A ladder-shaped radiator with a C-shaped slit inserted on the ground plane makes up the antenna's monopole radiator. A compact antenna is proposed in this paper with dimensions of $0.076\,\lambda \times 0.409\,\lambda \times 0.005\,\lambda$. This achieves dual band characteristics, which cater to 3.5/5.5 GHz (WiMAX), 5.8 GHz (WLAN), 6.3 GHz (C-band), and sub-6 GHz 5G bands. For the available aperture, reasonable gain is attained by the proposed architecture. Furthermore, fractional bandwidth of 69% and 43% in 2.6 GHz and 5.5 GHz bands, respectively, acting in accordance with the bandwidth stated by Wheeler and Chu's limit, has been attained in this ACS-fed antenna. In both the operating frequency bands, more than 20 dB isolation between the antenna elements has been achieved. High integrity is attained by the radiation pattern, and actual deployment is granted. Moreover, the simulated results presented are in good accordance with the measured results.

1. Introduction

The dramatic increase in global mobile data traffic in recent years because of various advanced applications, including the Internet of Things (IoT), wearable devices, and 5G communication, put a lot of pressure on upgradation of communication systems in terms of capacity and performance. The spectrum in sub-6 GHz bands is covered by a wide range of commercial wireless standards, such as WLAN (wireless local area network), worldwide interoperability for WiMAX (microwave access), and C-band applications [1]. Portable devices with multicarrier hardware ecosystems have been created and tailored to target consumer applications [2], such as wireless sensor network nodes, wireless dongles, and IOT (Internet of Things) sensors [3–5]. The data rates are still limited in sub-6 GHz communication because of the narrow bandwidth. The network at the spectrum level must seamlessly utilize sub-6 GHz bands for the spatial multiplexing and coverage of many devices. In contrast, higher bands must be employed for expelling the peak rates of point-to-point links [6, 7]. The constraints while designing the above-mentioned applicants are critical as very compact radiators are required in low-power devices so that they fit in these devices. The antennas should be compact with the primary module consisting of the substrates of the RF boards and should support pattern diversity to achieve better device throughput. Antennas have specific and preferable resonances over the nonresonant UWB (ultrawideband) antennas [8]. A compact simple structure MIMO UWB antenna is proposed in [9] for portable devices. A connecting metal line and cross-shaped decoupling slots are engraved on the ground plane to attain UWB characteristics and separation/isolation between the elements. Here, we have proposed a composite right left

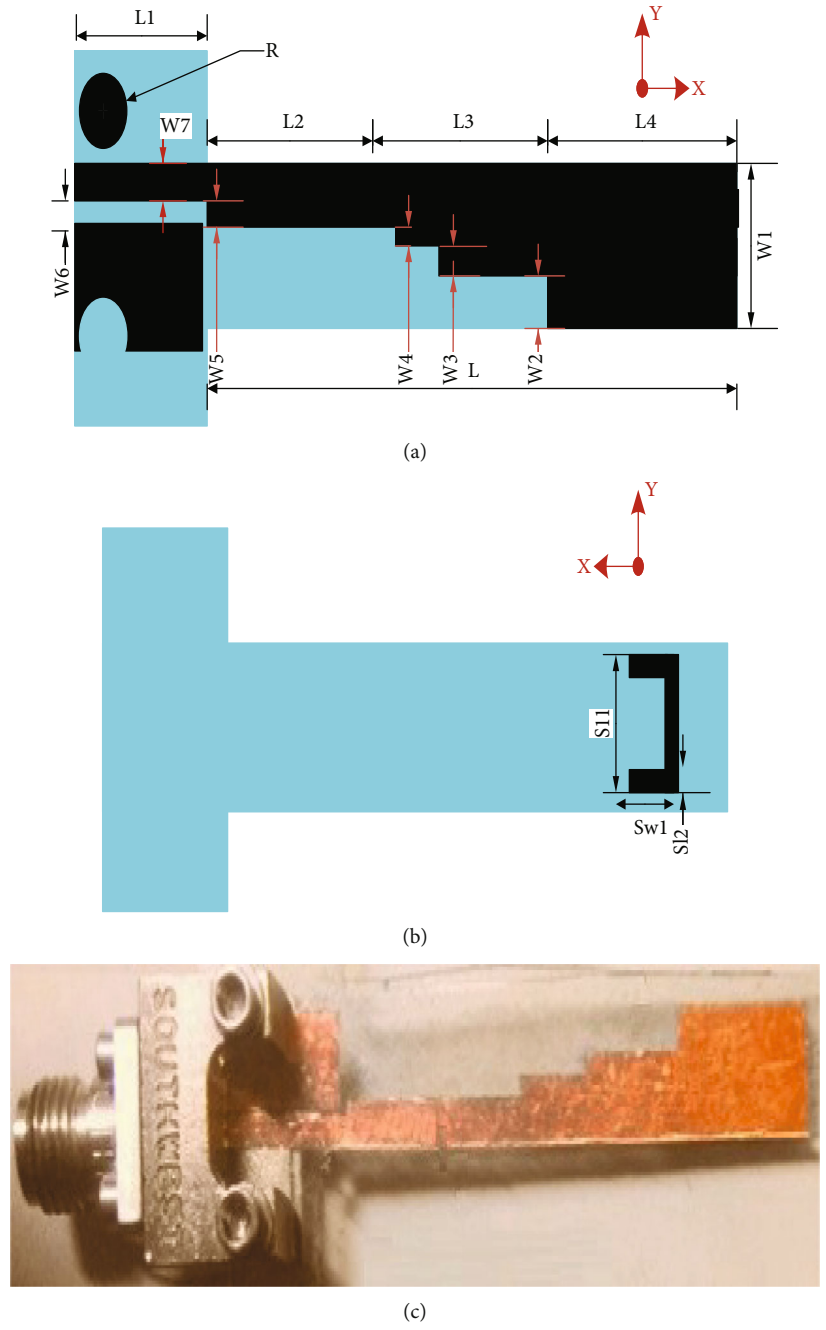

Figure 1: (a) Top side view. (b) Bottom side view. (c) Fabricated prototype.

handed (CRLH) MIMO antenna fed with an asymmetric coplanar strip for multiband operations with separation of $0.4\,\lambda_o$ at 5 GHz which is proposed in [10]. The antenna system achieves isolation of 25 dB and ECC lower than 0.05 without employing additional decoupling structures. Another structure with an ACS-fed antenna with a shared radiator is discussed for UWB applications [11]. The operating bandwidth is extended by introducing a rectangular patch on its back side and incorporating an I-shaped slot into the radiator. High isolation between the two antenna elements is realized. Few recent research papers on miniaturizing antennas and making them electrically small with multiband operations are discussed in [12–15]. Integrating MIMO antenna modules in handheld portable devices is quite difficult compared to single-element integration. Another finding is that the patterns should differ significantly with low isolation, which poses a difficult design problem in a low-frequency, electrically and spatially confined system.

2. Design, Analysis, and Performance of the Proposed Antenna

For band notching purposes, the proposed antenna comprises of an ACS-fed antenna with a split ring resonator

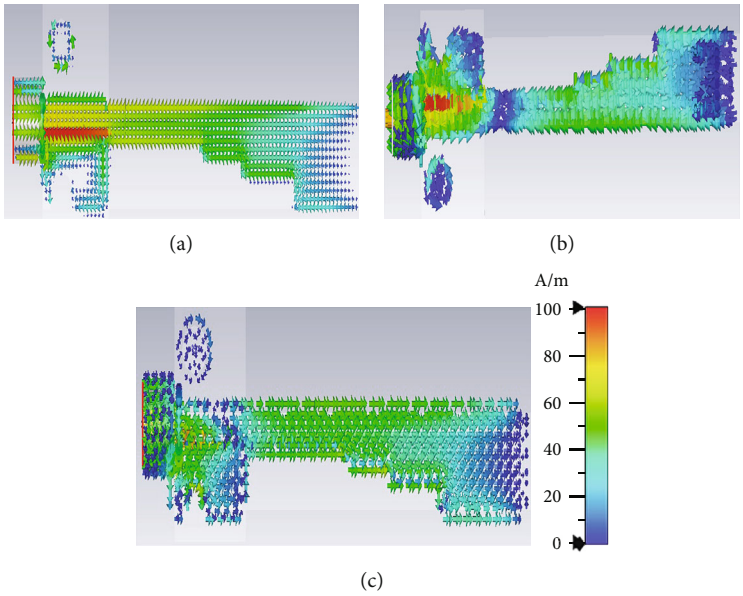

FIGURE 2: Surface current distributions at (a) 2.6 GHz, (b) 4.5 GHz, and (c) 5.5 GHz in the proposed scheme.

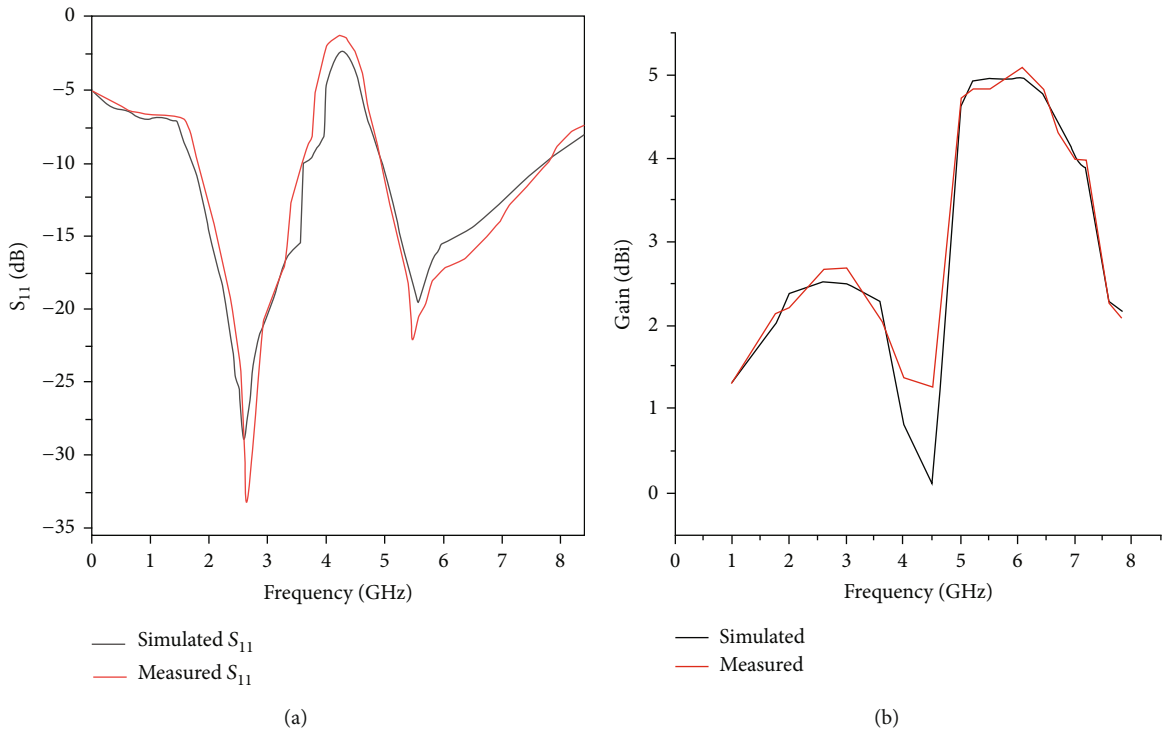

FIGURE 3: (a) Reflection coefficient (input). (b) Gain plot.

(SRR). A 20 mil Rogers 5880 substrate with a loss tangent of 0.01 and a dielectric constant (ε_r) of 2.2 have been basically used to design the proposed antenna. Computer simulation tool (CST) microwave studio is used for simulating the antenna. ACS feeding technique is considered the best technique for size reduction of an antenna as impedance matching is not affected while tuning the antenna, and it hardly affects the antenna efficiency. Furthermore, achieving multiband operations is easier than the techniques discussed earlier [13–16]. The proposed antenna structure schematics are displayed in Figure 1. Since the high dielectric constant of the substrate results in low radiation efficiency that is why to reduce the cross-polarization, a low dielectric constant thin substrate is chosen. The 50 Ω asymmetric coplanar strip feed line has a trace width of W6 and a W5 gap between the coplanar ground and signal trace, feeding the antenna structure. The antenna is compact with overall dimensions of $0.076\,\lambda \times 0.409\,\lambda \times 0.005\,\lambda$ at 2.6 GHz frequency. The

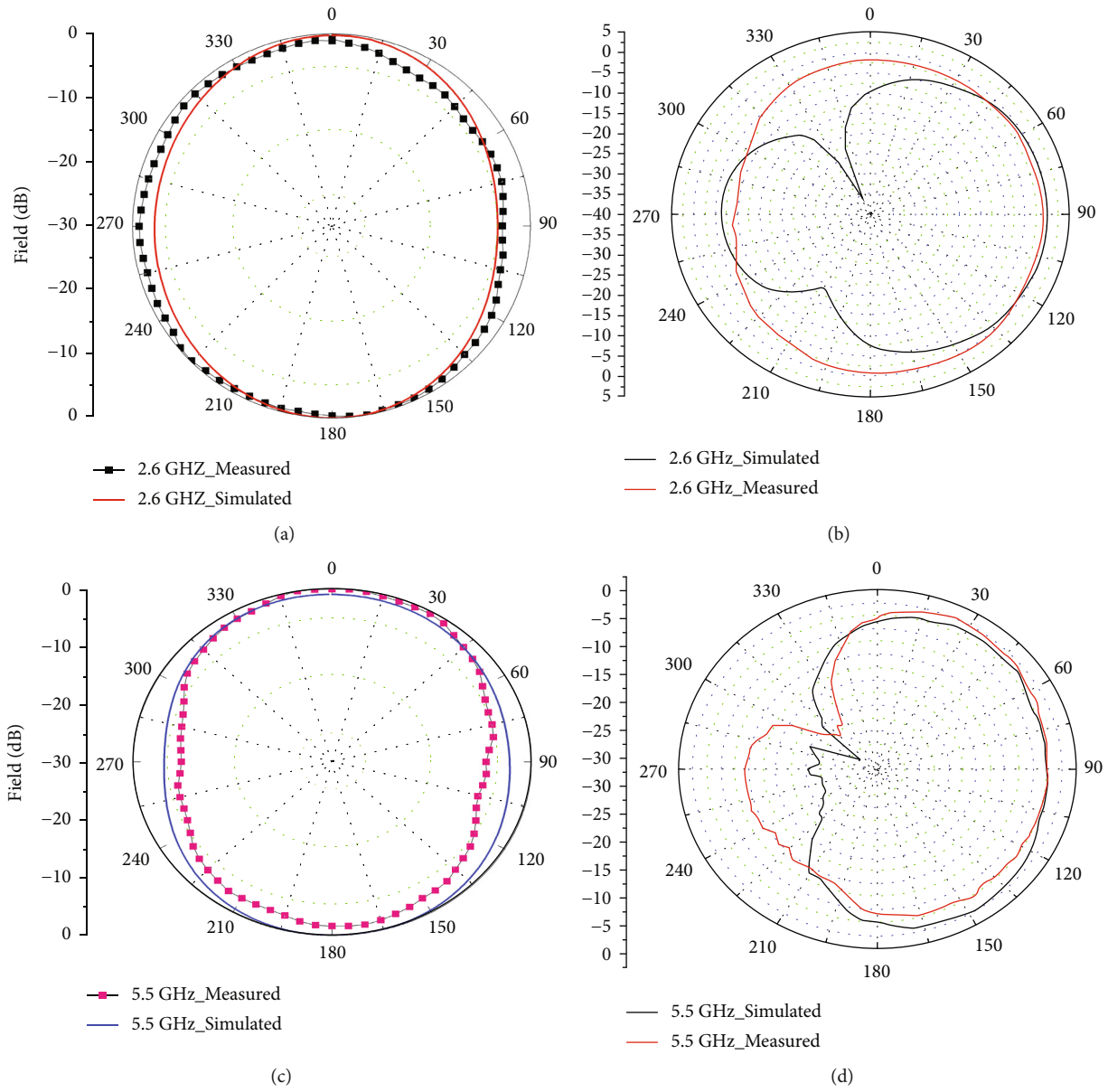

Figure 4: (a, c) 2.6 and 5.5 GHz cross-planar radiation patterns in *E*. (b, d) 2.6 and 5.5 GHz coplanar radiation pattern in *H* plane.

dimensions of the structure (in mm) are as follows: $L = 37$, $L1 = 10$, $L2 = 15$, $L3 = 15$, $L4 = 17$, $W1 = 8.8$, $W2 = 3.3$, $W3 = 1.8$, $W4 = 1.2$, $W5 = 1.0$, $W6 = 0.3$, and $W7 = 1.4$. The proposed antenna operated in the frequency ranges of 1.75-3.6 GHz and 5.0-7.7 GHz. Moreover, the structure is fabricated, the results are measured using Keysight FieldFox Microwave Analyzer N99518, and the results were found in good accordance with the simulated results. SMA connector cannot be used for measurement due to faulty soldering between the trace of the asymmetric coplanar strip antenna and the launch pin. As a result, a high frequency-appropriate end-launch connector is utilized. On both sides of the feed line, Rogers 5880 substrate is extended for mounting bulky end-launch connector having industry standard 2.92 mm, and high impedance bandwidth is achieved.

In UWB antennas, thus deployment of ladder-type changing structures in the radiator is incorporated for better broadband and impedance matching. The input reflection coefficient of the antenna depicts the same.

An open-end C-shaped split ring resonator (SRR) is introduced in the back side of the antenna in order to band notching frequencies. The SRR's length affects the frequency of notching, and for the proposed antenna, it is $2 \times Sw1 + Sl1$. At the notched frequency, that is roughly equivalent to the quarter wavelength. The ladder shape of the radiator also improves the impedance bandwidth. By introducing SRR, the antenna achieves the band notching characteristics at 4.5 GHz and dual pass band characteristics at 2.6 GHz and 5.5 GHz, which caters to 5G mid bands including NR n38 band, 3.5 GHz, and 5.5 GHz band suitable for WiMAX, 5.8 GHz band for WLAN, and C-band, i.e., 6.3 GHz.

In addition, to analyze and understand the proposed antenna© working mechanism, surface current distribution characterization is illustrated in Figure 2. Figures 2(a) and

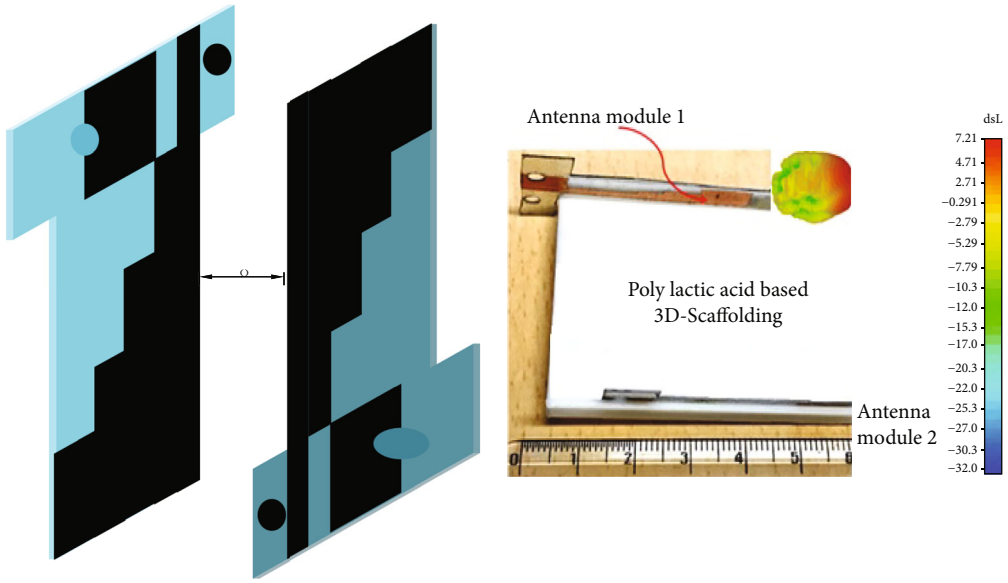

FIGURE 5: (a) Two-element flipped MIMO configuration. (b) Fabricated design.

2(c) show the current distribution at 2.6 and 5.5 GHz, respectively. The current in the radiator is dispersed equally between the two situations. However, the surface current concentration at the 4.5 GHz notched frequency range is mostly at the C-shaped open-ended slot. Because the currents flow in the opposite directions over this slot, destructive interference results in the band notching properties.

Figure 3(a) displays the designed ACS-fed antenna's simulated and measured input reflection coefficient. In order to cover the working frequencies of 1.75-3.6 GHz and 5.0-7.7 GHz, it achieves dual-passband characteristics at 2.6 GHz and 5.5 GHz. Tolerances in the fabrication process and the substrate's heterogeneous dielectric constant may be to responsible for differences between simulated and measured findings.

For the lower band and upper band, the proposed antenna's fractional bandwidths are 69% and 43%, respectively. The work of Wheeler [15] and Chu [16] is generally considered for the investigation of small miniaturized antennas. The work establishes theoretical limits showing how bandwidth and electrical size are related to each other. Collin and Rothschild [17] used the work in [15, 16] to develop an expression for the lowest quality factor (Q), and they approached the issue by deducting radiation-related energy from the overall energy. According to the authors, the electrical size of the antenna's lowest order mode is equal to

$$Q = \frac{1}{ka} + \frac{1}{(ka)^3}, \tag{1}$$

where $k = 2\pi/\lambda$ and a is antenna's minimum enclosing spherical area.

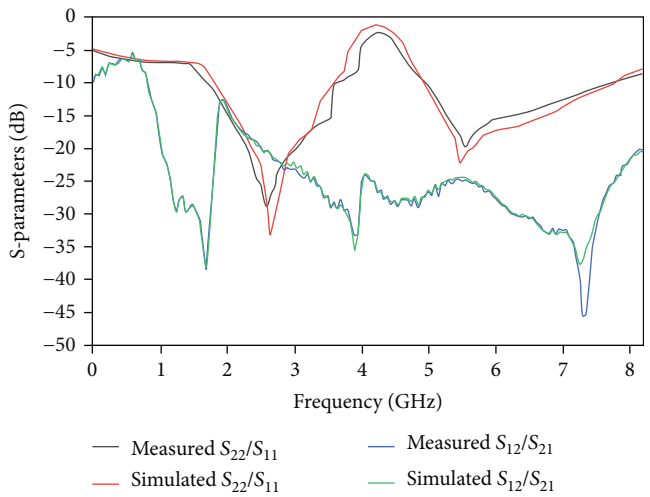

FIGURE 6: Simulated and measured reflection coefficient and isolation.

In [18], the authors calculated Q involving both TE and TM modes together for circularly polarized antennas as

$$Q = \frac{1}{ka} + \frac{1}{2(ka)^3}. \tag{2}$$

The relationship between $Q_{\min}$ and bandwidth (B) was derived by Yaghjian and Best [19] and is given as

$$B = \frac{1}{Q}\frac{\Gamma - 1}{\sqrt{\Gamma}}, \tag{3}$$

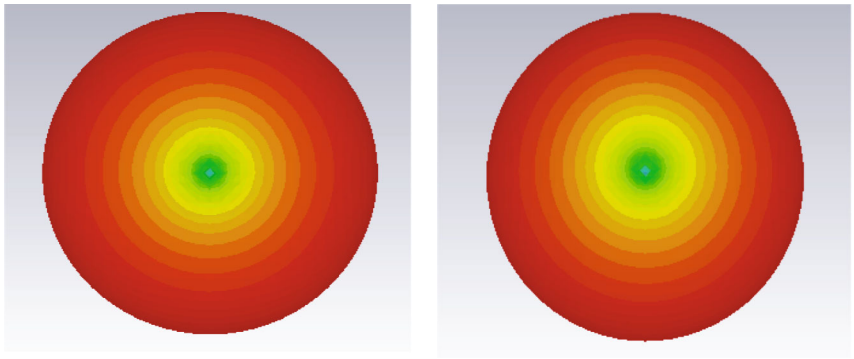

(a) (b)

Figure 7: 3D radiation pattern at (a) 2.6 GHz and (b) 5.5 GHz in XY plane.

where the antenna's maximum permitted VSWR is Γ. For small antennas, the sphere needs to completely cover the ground plane and radiator. Thus, at the resonant frequency in the lower band for this suggested antenna, a is 9 mm and k is 82.3 rad/m. Equations (2) and (3) show that the theoretically permitted maximum bandwidth is 72% larger than the experimentally determined fractional bandwidth. As a result, the proposed antenna falls under the electrically compact and small antenna category [20–22].

As shown in Figure 3(b), the proposed antenna's peak gains for the lower band and upper band are 2.5 dBi and 4.8 dBi, respectively. Figure 4 displays the cross-planar and coplanar simulated and measured radiation patterns in XY planes at 2.6 GHz and 5.5 GHz. In H plane at both frequencies, antenna achieves omnidirectional radiation pattern. Both inadequate absorptivity inside the anechoic chamber and stray current flowing beyond the cable and connector may contribute to differences between the measured and simulated radiation.

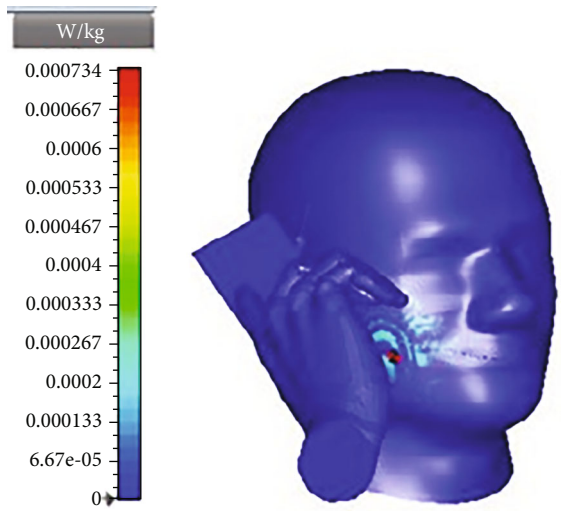

Figure 8: Investigated specific absorption rate (SAR) at 2.6 GHz.

3. Ladder-Shaped ACS-Fed Antenna for MIMO Applications

For antenna in MIMO configuration, the same single-element ACS-fed antenna that was explained in the previous section is utilized. The structure proposed is placed on the opposite edges of the smartphone. The MIMO configuration is obtained by flipping the structure on the other side as shown in Figure 5.

The elements are placed at proper distance so that the configuration meets the standards for the smartphone dimensions as depicted in Figure 5. While obtaining the results, one port is excited, and the other port is simultaneously terminated. The reflection coefficients and the isolation are shown in Figure 6. The radiation plots for both at 2.6 GHz and 5.5 GHz are shown in Figures 7(a) and 7(b), respectively.

In order to evaluate the radiation properties of an antenna system for a smartphone application, specific absorption rate (SAR) is used to forecast the effects of radiations on the human head. It can be seen as a function that assesses the amount of electromagnetic radiation that human tissue is exposed to when receiving and sending RF signals. SAR is thought to be a major worry for smartphone antenna systems, and for safer handling, the devices must have very low levels. SAR can be mathematically calculated as follows:

$$\text{Specific absorption rate (SAR)} = \frac{\sigma |E|^2}{2\rho}, \tag{4}$$

where σ represents the electrical conductivity, ρ represents the current density of biological tissue, and $|E|$ is the maximal value of electric field induced in the human tissues. The SAR values determine the harmful effects of electromagnetic radiation on human tissues. According to the IEEE C95.1:2005, which established the safety limitations, if the SAR values are higher than 2 W/kg per 10 g of tissue, it is thought to be extremely damaging to the human body. Thus, the SAR value needs to be as low as possible as the mentioned limit [23] between the mobile antenna and the human head. Figure 8 depicts the induced values of specific absorption rate (SAR) inside the body. Furthermore, incident power density is given by $E^2/377$.

The degree of the correlation between the elements is described in terms of ECC (envelope correlation coefficient),

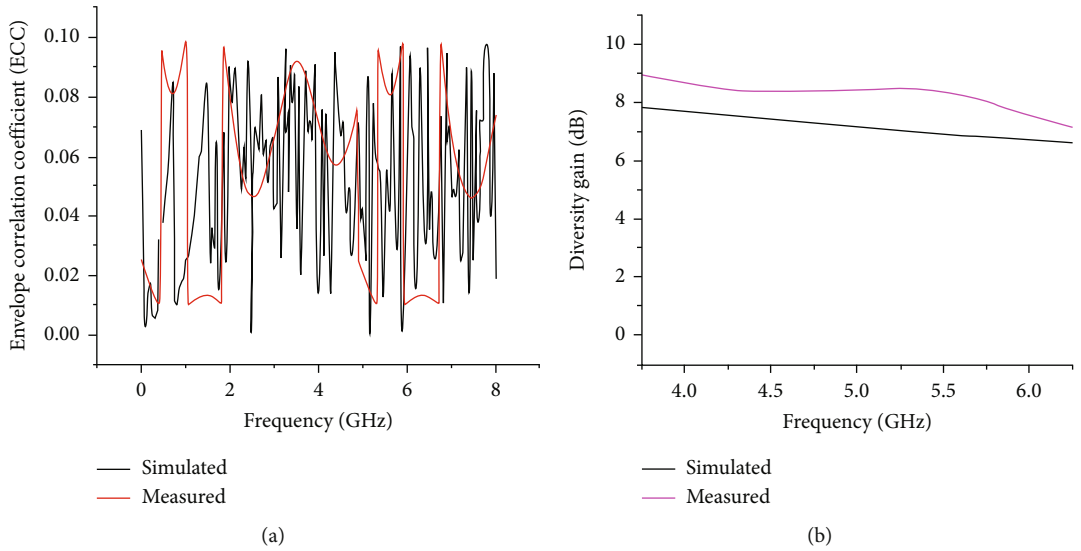

Figure 9: Simulated and measured values of ECC and DG for the proposed structure.

Table 1: Comparison of the designed antenna with various recently published state of art papers.

Ref.	Antenna size (mm^2)	Operating frequency (GHz)	Type of feeding	Isolation (dB)	Peak gain (dBi)	ECC
[6]	$0.38\,\lambda_o \times 0.38\,\lambda_o$	3.1-11	ACS	-15	3.5	<0.005
[7]	$0.476\,\lambda_o \times 0.485\,\lambda_o$	5/5.8/6.3	ACS	-18	N.A	<0.21
[8]	$0.204\,\lambda_o \times 0.39\,\lambda_o$	3.1–10.6	ACS	-15	3.5	N.A
[9]	$0.4\,\lambda_o \times 0.7\,\lambda_o$	4.6/4.9/5.4	ACS	-25	N.A	<0.02
[10]	$0.2\,\lambda_o \times 0.208\,\lambda_o$	2.5/5.6	Microstrip	-20	0.28/3.88	<0.004
[11]	$0.422\,\lambda_o \times 0.06\,\lambda_o$	2.4/5	Microstrip	-15	N.A	<0.2
[12]	$0.128\,\lambda_o \times 0.23\,\lambda_o$	3.5/5.5/5.8/6.3	ACS	-15	3.3/3.5/3.9/3	<0.02
[24]	$0.612\,\lambda_o \times 0.612\,\lambda_o$	3.65/4.75/9.10	CPW	-15	4	<0.17
[25]	$0.375\,\lambda_o \times 0.316\,\lambda_o$	2.5/3.6/5.5	Microstrip	-18	5	<0.04
[23]	$1.65\,\lambda_o \times 1.65\,\lambda_o$	5.5/6.75	CPW	-25	3.5/4	<0.008
This Work	$0.076\,\lambda_o \times 0.409\,\lambda_o$	1.75-3.6/5.0-7.7	ACS	-20	2.5/4.8	<0.09

which is regarded as a crucial metric when building MIMO antenna systems. Authors massively adopt ECC to estimate the MIMO antenna system diversity performance. In order to transmit data streams simultaneously and independently, the antenna radiators must attain weak. Equation (5) is used to calculate for an N-port MIMO antenna system.

$$\rho_e(i,j,N) = \left| \frac{\sum_{n=1}^{N} S_{i,n}^{*} S_{n,j}}{\left| \prod_{k=i,j} \left(1 - \sum_{n=1}^{N} S_{k,n}^{*} S_{n,k}\right) \right|^{1/2}} \right|^2, \quad (5)$$

where ρ_e represents correlation among two antenna elements and the number of antenna elements is given by N.

The surge in signal to interference ratio in a MIMO antenna system while consolidating different diversity schemes is discussed by the important parameter DG (diversity gain). DG of an antenna system is dependent on correlation coefficient (ρ_e). Equation (6) is applied to calculate the DG of a MIMO antenna system.

$$DG = 10 \times \sqrt{1 - |\rho_e|}. \quad (6)$$

The diversity gain (DG) and envelope correlation coefficient (ECC) of the two-port MIMO antenna is shown in Figures 9(a) and 9(b), respectively. It is evident from the figure that the value of ECC is less than 0.1 dB denoting the isolation is good between the MIMO antenna elements. In the operating band, the measured value of diversity gain is touching 9 dB. Therefore, the MIMO antenna system that has been proposed is having acceptable diversity performance.

Furthermore, Table 1 presents the table of comparison between the designed antenna and other state of art.

4. Conclusion

An electrically compact ACS-fed antenna integrated in smartphone with actual dimensions of $0.076\,\lambda \times 0.409\,\lambda \times 0.005\,\lambda$ is proposed, designed and fabricated successfully over Rogers RT 5880 substrate. The antenna provides the dual-passband characteristics which cater to WiMAX, WLAN, C-band and sub-6 GHz 5G bands and achieves the FBW (fractional bandwidth) of 69% and 43% in both the upper and lower bands, respectively. The MIMO of the prototype is also discussed achieving orthogonal pattern diversity. The MIMO configuration has respectable values of ECC and diversity gain. The antenna serves as potential candidate for 5G and IoT application considering the boom in capacity and increased data rates.

Data Availability

No underlying data was collected or produced in this study.

Conflicts of Interest

The authors declare that they have no conflicts of interest.

Acknowledgments

This work has been supported by the Department of Science and Technology (DST) ICPS Scheme under Grant No. DST/ICPS/CLUSTER/IOT/2018/General and hence acknowledges the funding agency. The authors highly acknowledge the contribution and mentorship of Late Prof. G. Mohiuddin Bhat who lost his life due to the COVID-19 pandemic while guiding us as he was part of the project work.

References

[1] C. Rowell and E. Y. Lam, "Mobile-phone antenna design," *IEEE Antennas and Propagation Magazine*, vol. 54, no. 4, pp. 14–34, 2012.

[2] K.-L. Wong, S.-W. Su, C.-L. Tang, and S.-H. Yeh, "Internal shorted patch antenna for a UMTS folder-type mobile phone," *IEEE Transactions on Antennas and Propagation*, vol. 53, no. 10, pp. 3391–3394, 2005.

[3] X. Shi, M. Zhang, S. Xu, D. Liu, H. Wen, and J. Wang, "Dual-band 8-element MIMO antenna with short neutral line for 5G mobile handset," in *2017 11th European Conference on Antennas and Propagation (EUCAP)*, pp. 3140–3142, Paris, France, 2017.

[4] K. L. Wong, B. W. Lin, and B. W. Y. Li, "Dual-band dual inverted-F/loop antennas as a compact decoupled building block for forming eight 3.5/5.8-GHz MIMO antennas in the future smartphone," *Microwave and Optical Technology Letters*, vol. 59, no. 11, pp. 2715–2721, 2017.

[5] S. Koziel, S. Ogurtsov, W. Zieniutycz, and A. Bekasiewicz, "Design of a planar UWB dipole antenna with an integrated balun using surrogate-based optimization," *IEEE Antennas and Wireless Propagation Letters*, vol. 14, pp. 366–369, 2015.

[6] H. Qin and Y.-F. Liu, "Compact UWB MIMO antenna with ACS-fed structure," *Progress In Electromagnetics Research C*, vol. 50, pp. 29–37, 2014.

[7] A. A. Ibrahim, M. A. Abdalla, and Z. Hu, "Compact ACS-fed CRLH MIMO antenna for wireless applications," *IET Microwaves, Antennas & Propagation*, vol. 12, no. 6, pp. 1021–1025, 2018.

[8] J.-Y. Zhang, F. Zhang, W.-P. Tian, and Y.-L. Luo, "ACS-fed UWB-MIMO antenna with shared radiator," *Electronics Letters*, vol. 51, no. 17, pp. 1301-1302, 2015.

[9] M. A. Abdalla, D. Z. Nazif, and A. M. Ali, "Two elements MIMO antenna with asymmetric coplanar strip metamaterial configuration and EBG hybrid isolation," in *2018 12th International Congress on Artificial Materials for Novel Wave Phenomena (Metamaterials)*, pp. 001–003, Espoo, Finland, 2018.

[10] S. Nandi and A. Mohan, "A compact dual-band MIMO slot antenna for WLAN applications," *IEEE Antennas and Wireless Propagation Letters*, vol. 16, pp. 2457–2460, 2017.

[11] J. Deng, J. Li, L. Zhao, and L. Guo, "A dual-band inverted-F MIMO antenna with enhanced isolation for WLAN applications," *IEEE Antennas and Wireless Propagation Letters*, vol. 16, pp. 2270–2273, 2017.

[12] H. Wong, K. K. So, K. B. Ng, K. M. Luk, C. H. Chan, and Q. Xue, "Virtually shorted patch antenna for circular polarization," *IEEE Antennas and Wireless Propagation Letters*, vol. 9, pp. 1213–1216, 2010.

[13] D. Wang, H. Wong, and C. H. Chan, "Small patch antennas incorporated with a substrate integrated irregular ground," *IEEE Transactions on Antennas and Propagation*, vol. 60, no. 7, pp. 3096–3103, 2012.

[14] N. Amani and A. Jafargholi, "Zeroth-order and TM_{10} modes in one-unit cell CRLH mushroom resonator," *IEEE Antennas and Wireless Propagation Letters*, vol. 14, pp. 1396–1399, 2015.

[15] H. A. Wheeler, "Fundamental limitations of small antennas," *Proceedings of the IRE*, vol. 35, no. 12, pp. 1479–1484, 1947.

[16] L. J. Chu, "Physical limitations of omni-directional antennas," *Journal of Applied Physics*, vol. 19, no. 12, pp. 1163–1175, 1948.

[17] R. Collin and S. Rothschild, "Evaluation of antenna Q," *IEEE Transactions on Antennas and Propagation*, vol. 12, no. 1, pp. 23–27, 1964.

[18] J. S. McLean, "A re-examination of the fundamental limits on the radiation Q of electrically small antennas," *IEEE Transactions on Antennas and Propagation*, vol. 44, no. 5, p. 672, 1996.

[19] A. D. Yaghjian and S. R. Best, "Impedance, bandwidth, and Q of antennas," *IEEE Transactions on Antennas and Propagation*, vol. 53, no. 4, pp. 1298–1324, 2005.

[20] R. Song, G.-L. Huang, C. Liu et al., "High-conductive graphene film based antenna array for 5G mobile communications," *International Journal of RF and Microwave Computer-Aided Engineering*, vol. 29, no. 6, Article ID e21692, 2019.

[21] R. N. Tiwari, P. Singh, and B. K. Kanaujia, "A compact UWB MIMO antenna with neutralization line for WLAN/ISM/ mobile applications," *International Journal of RF and Microwave Computer-Aided Engineering*, vol. 29, no. 11, article e21907, 2019.

[22] R. N. Tiwari, P. Singh, B. K. Kanaujia, and P. Kumar, "Compact circularly polarizedMIMOprinted antenna with novel ground structure for wideband applications," *International Journal of RF and Microwave Computer-Aided Engineering*, vol. 31, no. 8, article e22737, 2021.

[23] J. Kulkarni, C. Y. D. Sim, A. Desai et al., "A compact four port ground-coupled CPWG-fed MIMO antenna for wireless applications," *Arabian Journal for Science and Engineering*, vol. 47, no. 11, pp. 14087–14103, 2022.

[24] N. P. Kulkarni, N. B. Bahadure, P. D. Patil, and J. S. Kulkarni, "Flexible interconnected 4-port MIMO antenna for sub-6 GHz 5G and X band applications," *AEU-International Journal of Electronics and Communications*, vol. 152, article 154243, 2022.

[25] J. Kulkarni, A. G. Alharbi, I. Elfergani, J. Anguera, C. Zebiri, and J. Rodriguez, "Dual polarized, multiband four-port decagon shaped flexible MIMO antenna for next generation wireless applications," *IEEE Access*, vol. 10, pp. 128132–128150, 2022.